UNIVERSITÀ DEL PIEMONTE ORIENTALE

School of Medicine

Health Sciences Department

Master's Degree in Medical Biotechnologies

The Sodium Ionophore Monensin Inhibits Hepatocarcinogenesis: Study in an Immunocompetent Mice Model of NAFLD-DEN Induced Hepatocellular Carcinoma

Academic year 2024/2025

Supervisor:

Prof.ssa Rita CARINI

Candidate:

Abdulsalam ASHKAR

Index

Acknowledgement

Grateful acknowledgement is extended to Professor Umberto Dianzani and his team at the Università del Piemonte Orientale for their valuable collaboration in this project. Their technical expertise and support in PCR analyses and blood sample processing contributed significantly to the experimental outcomes and scientific robustness of this study.

This work was supported by Associazione Italiana Ricerca sul Cancro (AIRC, Grants IG-2020-24351 to RC) by the Italian Ministry of Health (grant No RF-2018-12366471 to A.F.) and by Fondazione Cariplo (grant No. 2018-0253 to C.B.).

1. Summary

Rationale of the study: Hepatocellular carcinoma (HCC), the third leading cause of cancer-related deaths globally, lacks effective treatments for advanced stages. Monensin, a repurposed coccidiostat, demonstrates promising anti-tumor effects, yet remains understudied. Our prior work confirmed its safety and efficacy across multiple cancer models, including HCC, breast cancer (4T1), and melanoma (B16-F10) allografts, where it reduced tumor burden, suppressed angiogenesis, and boosted $CD8^+$ T cell infiltration—all while sparing healthy cells. This thesis advances these findings by testing monensin in a translational Diethylnitrosamine-induced NAFLD-HCC model that recapitulates human disease progression.

Planning of the study: NAFLD-DEN induced HCC was obtained by intraperitoneally injecting C57BL/6 neonatal mice with a single DEN dose. Following the weaning period, the animals were maintained on a specialized Choline Deficient L-Amino Acid-Defined (CDAA). Immunohistochemical, Histopathological, and qPCR analysis were utilized to assess the intra-tumoral composition in control and treated mice. Tumor burden, neo-angiogenesis, steatosis, immune infiltration, and inflammation were evaluated by cell density, CD31, lipid accumulation, immune cells' markers, and mRNA of interleukins and cytokines, respectively. In vitro investigation of monensin potential included sodium dependency, intracellular lipid accumulation, and proliferation inhibition, using imaging techniques and Western Blot assay.

Results: Monensin treated mice exhibited significantly reduced tumor burden, evident by reduced nodules count, mass, and cell density. In addition, monensin reduced neo-angiogenesis, and steatosis, while showing elevated immune infiltration and proinflammatory microenvironment. This selective activity against cancer cells was not mediated by anti-proliferative effects, and it was sodium dependent.

Conclusion: These results establish monensin as a multi-action anti-HCC agent, targeting tumor vasculature while boosting anti-tumor immunity. Its selectivity and safety support further development, particularly in combination with immunotherapies and targeted therapies. Additionally, its anti-steatosis activity requires further charectrization.

2. Introduction

2.1. Epidemiology and aetiology

Liver cancer ranks as the sixth most frequently diagnosed cancer globally, with 866,136 new cases reported in 2022, and it stands as the third leading cause of cancer-related deaths worldwide, accounting for 758,725 fatalities. In Italy, 11,886 cases were diagnosed in 2022, leading to 9,606 deaths, with incidence rates increasing with age [1]. Hepatocellular Carcinoma (HCC) is observed in approximately 90% of liver malignancies [2].

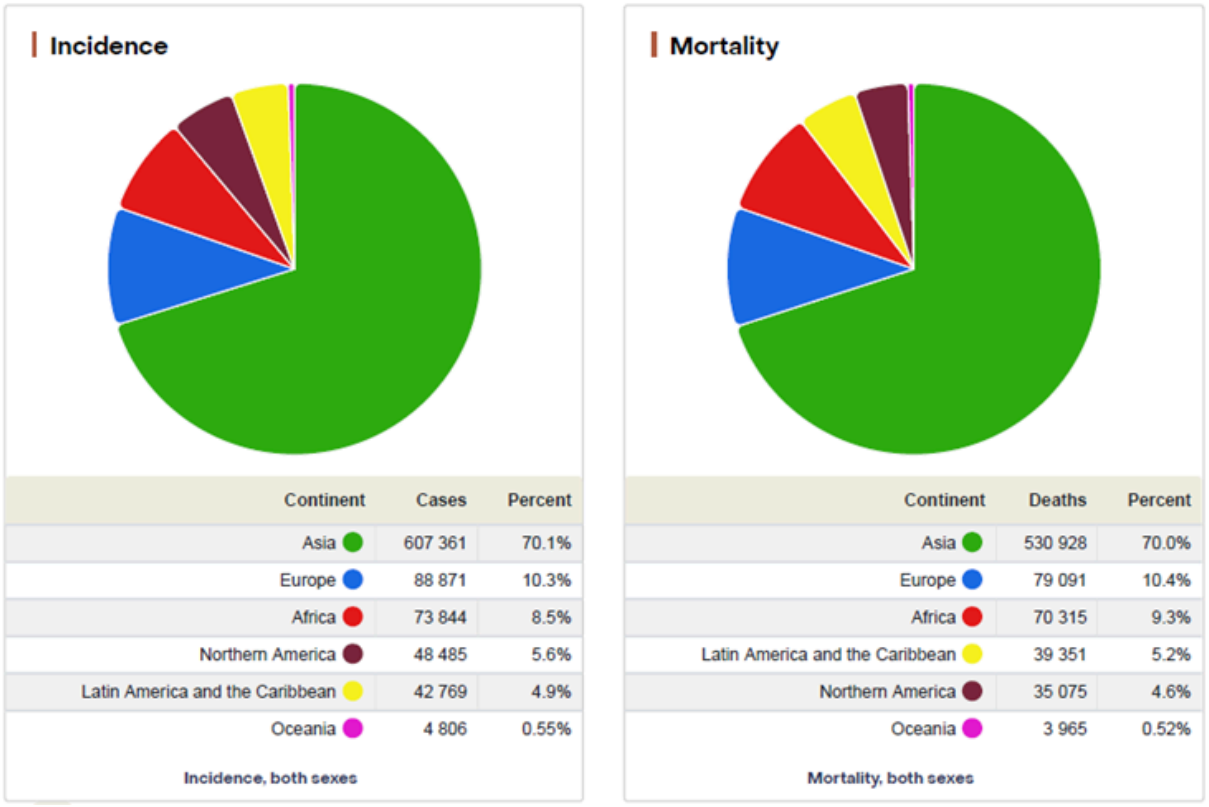

Figure 1: Estimated global distribution of liver cancer incidence and mortality in 2022

The pie charts illustrate the global incidence of liver cancer and its mortality in the different continents.

The global epidemiology of HCC is undergoing a significant shift, with incidence projected to rise steadily over the next three decades. This trend reflects changing risk factors: while hepatitis B (HBV) and C (HCV) infections—traditionally major drivers of HCC—are

declining, Non Alcoholic Fatty Liver Disease (NAFLD) is becoming increasingly prevalent. The surge in NAFLD cases is so substantial that it outweighs the reduction in viral hepatitis-related HCC (Fig. 2), leading to a net increase in overall incidence [3]. Similar trends are being observed globally, mostly attributed to increasing obesity, diabetes, and nonalcoholic steatohepatitis (NASH) prevalence.

HBV infection was widely regarded as the most common risk factor for HCC. However, HBV vaccination and treatments for HBV and HCV are considered preventive measures. The use of Direct-Acting Antiviral (DAA) therapy has successfully treated an increasing number of HCV-infected patients, leading to a sustained virologic response (SVR) and reducing the risk of HCC by 50–80% [2].However, up to 25% of HCC cases occur in patients without a history of cirrhosis or its associated risk factors [4].

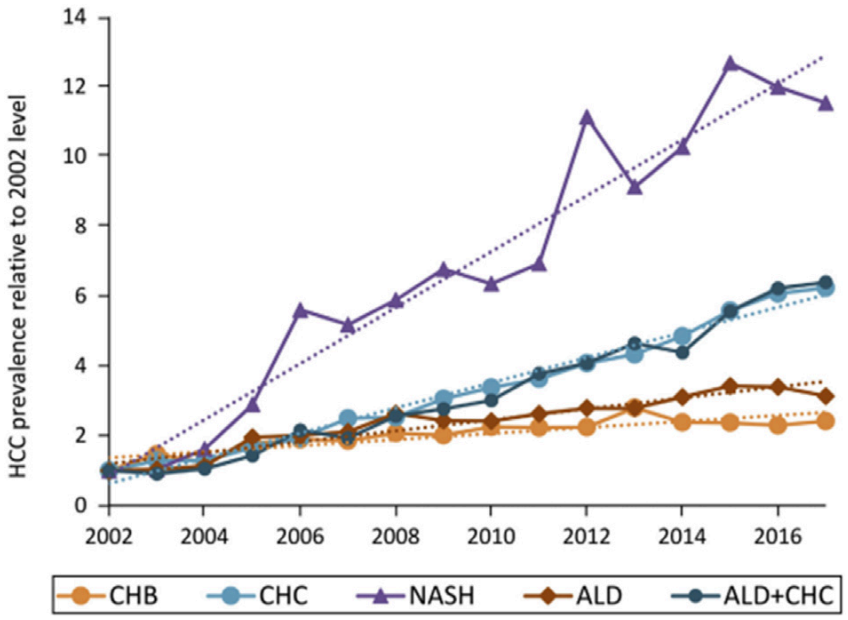

Figure 2: Shifts in HCC etiology trends from 2002 till 2016 in the USA

CHB: chronic hepatitis B; CHC: chronic hepatitis C; NASH: non-alcoholic Steatohepatitis; ALD: alcohol-associated liver disease [3].

2.2. NAFLD progression toward HCC

NAFLD represents the most widespread form of chronic liver pathology globally, and it is estimated to affect 25% of the global population. It encompasses a clinical spectrum

beginning with hepatic steatosis advancing to NASH. NASH is the fastest evolving leading cause of HCC, especially in Western countries. If left unmanaged, NASH can further deteriorate into hepatic fibrosis, cirrhosis, and eventually HCC (Fig. 3) [5]. In NASH-related cirrhosis, the annual incidence of HCC ranges from 0.5% to 2.6%, while in non-cirrhotic NAFLD, it is 0.01–0.13% per year. Even though the incidence of developing HCC from NAFLD is lower than developing it from viral hepatitis, the prevalence of viral hepatitis is much less than the prevalence of NASH [6].

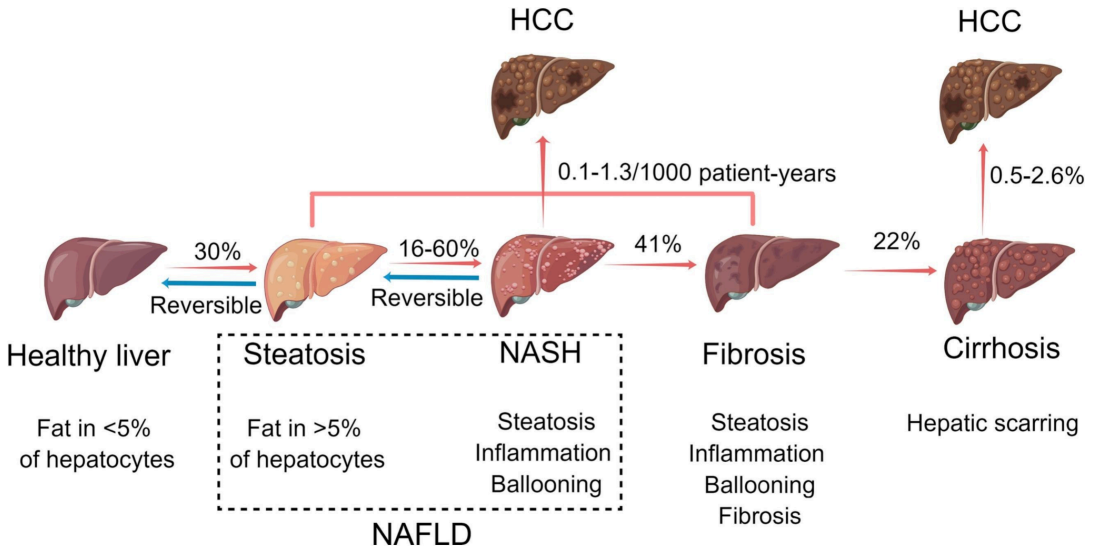

Figure 3: Stages of liver pathologies during developing NAFLD-related HCC

2.3. Genomic alterations underlying HCC

The molecular mechanisms underlying HCC vary based on specific genotoxic triggers and etiological factors. Despite advances in understanding the disease's pathophysiology and key drivers, clinical application remains limited. Approximately 25% of HCC tumors harbor mutations that could be targeted by therapies; however, the frequency of most of these mutations is below 10%, posing challenges for proof-of-concept studies. Key mutational drivers in HCC, such as TERT, TP53, and CTNNB1, remain difficult to target with current drug treatments [2]. Telomerase activation, often driven by TERT promoter mutations, viral insertions, chromosomal translocations, or gene amplification, is one of the most prevalent driver gene alterations, occurring in approximately 80% of HCC cases. Additionally, CCNA2 and CCNE1 may undergo oncogenic activation due to HBV or adeno-associated virus 2 [2,7,8].

Activation of the Wnt–β-catenin signaling pathway was observed in 30–50% of cases, primarily due to alterations in CTNNB1 (encoding β-catenin) or inactivation of AXIN1 or APC, which are inhibitors of the Wnt pathway. Genes involved in cell cycle regulation, such as TP53, RB1, CCNA2, CCNE1, PTEN, ARID1A, ARID2, RPS6KA3, and NFE2L2, were frequently found to be mutated or altered in HCC [8–10]. The most common mutations in HCC include TERT promoter, TP53, CTNNB1, AXIN1, ARID1A, and ARID2, collectively accounting for more than 90% of cases [11].

2.4. Clinical manifestations and diagnosis

HCC often progresses silently, making early detection difficult. In cirrhotic patients, reduced liver reserve leads to symptoms of decompensation such as jaundice, encephalopathy, ascites, or variceal bleeding, often associated with portal invasion. Non-cirrhotic patients, more common in high-incidence areas, present with advanced symptoms including cachexia, abdominal pain, hepatomegaly, or jaundice due to unrestricted tumor growth. Rarely, tumor rupture can cause acute pain, peritoneal irritation, and hypotension. HCC can also present with metastases, commonly to the bone, lungs, and abdominal organs, or with rare paraneoplastic effects such as hypoglycemia, diarrhea, or cutaneous signs. Porphyria cutanea tarda, linked to hepatitis C, is associated with an increased risk of HCC [12].

Alpha-fetoprotein (AFP) levels in adults are typically less than 10 ng/dL; elevated concentrations may indicate malignancies originating from the same endodermal lining as the hepatic diverticulum, such as the stomach and pancreas. AFP specificity is nearly 100% (minimal false positives), but its sensitivity is low, thus, less than 50% of patients develop diagnostic levels of AFP (400–500 ng/mL) (high false negatives), with 30% of patients showing normal serum levels of AFP at the time of diagnosis [13]. Ultrasound imaging, which may replace or be combined with AFP, can increase the Positive Predictive Value to 94% and is also effective in detecting masses smaller than 3 cm [12]. Ultrasonography (US), with or without AFP, is recommended for screening cirrhotic and high-risk patients, typically every six months, and to confirm the results from the ultrasonography, multiphase computed tomography (CT), magnetic resonance imaging (MRI), and potentially a biopsy can be indicated.

In recently diagnosed patients, complete blood cell count (CBC), electrolyte levels, liver function tests (LFTs), and coagulation tests are necessary to evaluate the severity of the case. Non-invasive imaging can be sufficient to establish a diagnosis, independently of biopsy confirmation, although imaging is required for guidance when a biopsy is needed [4]. The International Consensus Group for Hepatocellular Neoplasia has identified key histological characteristics of HCC, including stromal invasion, elevated cell density, intratumoral portal tracts, unpaired arteries, pseudo-glandular architecture, and widespread fatty changes [14]. For staging and management, the Barcelona Clinic Liver Cancer (BCLC) staging system and the National Comprehensive Cancer Network (NCCN) guidelines are widely endorsed [15].

2.5. Therapeutic approaches

2.5.1. Surgical and locoregional approaches

Surgical resection and Orthotopic Liver Transplantation (OLT) are the primary treatments for early-stage HCC, yet more than 90% of patients are not compatible with these options. Consequently, catheter-based and percutaneous locoregional therapies have become crucial alternatives for managing unresectable HCC. These therapies include Trans-Arterial Embolization (TAE), which involves blocking the blood supply to the tumor, Trans-Arterial Chemo-Embolization (TACE), which combines chemotherapy with embolization and is effective for tumors 3–5 cm in size, and Trans-Arterial Radio-Embolization (TARE), which delivers radiation directly to the tumor through the blood vessels, as well as ablative therapies. Ablation can be performed using different techniques, including Radio-Frequency Ablation (RFA), Microwave Ablation (MWA), Cryoablation (CA), Irreversible Electroporation (IRE), Laser-Induced Interstitial Thermotherapy (LITT), and High-Intensity Focused Ultrasound (HIFU), each with different criteria for patient selection, goals, outcomes, and complications [16].

2.5.2. Targeted approach

Anti-angiogenic treatments primarily target Vascular Endothelial Growth Factor (VEGF), offering synergistic effects when combined with immunotherapy. Bevacizumab and ramucirumab are monoclonal antibodies that target VEGF-A and VEGFR-2, respectively.

The Phase III REACH-2 trial evaluated 292 HCC patients with disease progression after sorafenib, (a tyrosine kinase inhibitor that targets pathways such as Ras/Raf/MAPK and VEGF) first-line treatment, showing that patients receiving ramucirumab had improved overall survival (8.5 vs. 7.3 months, HR 0.71, 95% CI 0.531–0.949), higher objective response rates (5% vs. 1%), and better disease control (60% vs. 39%) compared to placebo.

Apatinib, an anti-angiogenic tyrosine kinase inhibitor targeting VEGFR-2, achieved similar results to the previous drugs in phase III clinical trials. The SHARP trial demonstrated improved survival (10.7 vs. 7.9 months) and progression delay (5.5 vs. 2.8 months) in HCC patients, while the ORIENTAL trial confirmed similar benefits (6.5 vs. 4.2 months OS). Sorafenib is particularly effective in HCV-related HCC, with the SHARP trial showing the greatest survival benefit in these patients (14 vs. 7.4 months). Lenvatinib, another multitarget TKi, targets VEGFR1-3, PDGFR, KIT, FGFR1-4, and RET, with results from trials similar to sorafenib. Regorafenib and cabozantinib, other derivatives, may benefit patients with progression after first-line sorafenib, while donafenib has better pharmacokinetics. Telomerase inhibition, which reduces cellular immortality, is another target; studies have shown that imetelstat (GRN163L), perifosine, KML001, and BIBR1532 can inhibit telomerase activity. GV1001 (hTERT 611–626), P540 (hTERT540-548), GX301, and Vx-001 potentially possess anti-tumor activity as immunotherapies targeting hTERT [11,17].

2.5.3. Immunotherapeutic approach

Several monoclonal antibodies are indicated in the management of HCC, including Immune Checkpoint Inhibitors (ICIs) such as anti-Programmed Death-Ligand 1 (anti-PD-L1) agents like atezolizumab and durvalumab, anti-PD-1 agents like camrelizumab, nivolumab, and pembrolizumab, and anti-Cytotoxic T-Lymphocyte Antigen 4 (anti-CTLA-4) agent tremelimumab [17].

Combinations of these agents with others have demonstrated superior impacts on overall survival compared to sorafenib, as seen in trials such as IMbrave150 (atezolizumab and bevacizumab), HIMALAYA and STRIDE (durvalumab and tremelimumab), and camrelizumab and rivoceranib (a selective tyrosine kinase inhibitor for VEGFR-2). Immune therapy can be combined with locoregional approaches or used following resection or ablation to treat residual disease [18]. A meta-analysis assessing 6,290 patients across eight

trials evaluated the effectiveness of targeted and immunotherapy as first-line treatments for HCC, showing that the combination of bevacizumab and atezolizumab resulted in superior overall survival (OS) compared to sorafenib (HR 0.58, 95% CI 0.42–0.80), nivolumab (HR 0.68, 95% CI 0.48–0.98), and lenvatinib (HR 0.63, 95% CI 0.44–0.89) [11]. This combination is currently the first-line treatment for unresectable or advanced disease [4]. Nonetheless, the modest increase in overall survival duration, along with the significant expenses and complex adverse reactions associated with these therapies, highlights a substantial gap in HCC treatment.

2.6. Pre-clinical models for HCC

2.6.1. In-vitro models

HCC human cancer cell lines like HepG2, originally derived from a Caucasian teenage male, are widely used but may not fully replicate HCC due to recent findings linking them to a hepatoblastoma-like tumor. Alternatives like C3A and HepaRG are now preferred, with C3A showing more hepatocyte-like characteristics and HepaRG providing insights into drug toxicity and carcinogenesis. Murine cell lines such as Hepa1-6, Hep-53.4, RIL-175, and TIBx are valuable for their genetic similarities to humans, with a key model being Hepa-1c1c7, derived from Hepa1, which is particularly important for its contribution to HCC research due to its ability to replicate key aspects of the disease more effectively than earlier murine models [19]. Organoids, which are 3D culture systems, mimic key physiological traits of their target organs, balancing in vitro flexibility with in vivo complexity, although they are costly, labor-intensive, and lack immune and vascular components [20].

2.6.2. In-vivo models

Orthotopic cancer cell injection is considered the most clinically relevant for studying HCC and liver metastasis, as it mimics real surgical scenarios and replicates the TME of human HCC. However, this method is expensive, complex, and requires careful selection of mice and precise placement of carcinoma cells. Two primary techniques are used: subserosal injection, where tumour cells are injected with Matrigel to prevent dispersion, and surgical orthotopic transplantation, which involves embedding a small tumour cube into the liver

tissue. Ectopic transplantation allows the acquisition of subcutaneous lesions [20]. While subcutaneous implantation of HCC cells in immunodeficient mice enables straightforward tumor monitoring, this model lacks translational relevance due to its non-physiological microenvironment, absence of functional immunity, and exclusion of liver-specific comorbidities like steatosis or fibrosis. The artificial stromal architecture fails to replicate hepatobiliary interactions critical for drug metabolism and metastasis, while immunodeficient hosts preclude study of tumor-immune crosstalk, a key factor in HCC progression and therapy response [21].

Additionally, exogenous cell lines often exhibit genetic drift, losing heterogeneity seen in patient tumors, and rarely metastasize, unlike orthotopic or diet-induced models that integrate metabolic and immune components of human HCC [2]. PDX models involve grafting fresh tumour tissues from patients onto immunosuppressed mice. Despite their advantages, including studying treatment-naïve and resistant strains, PDX models face limitations such as low success rates and limited immune system representation [22].

Chemically induced liver cancer models vary depending on the carcinogen employed, with diethylnitrosamine (DEN) being the most widely used in preclinical studies due to its potent genotoxicity. DEN intraperitoneal administration induces a series of changes, including inflammation, fibrosis, and the formation of nodules or precancerous lesions, which can take weeks to months to form malignant tumors. This eventually results in tumors characterized by abundant somatic single-nucleotide variants (SNVs) and minimal insertions, deletions, or copy-number alterations, consistent with its mutagenic action. Computational analysis of DEN-driven tumors reveals six COSMIC mutational signatures and recurrent oncogenic driver mutations, including activating Hras (C61), Braf (C584), Egfr (C254), and truncating Apc alterations (21% of carcinomas), which promote Wnt/β-catenin dysregulation and malignant progression [23].

DEN-induced HCC better resembles the human HCC poor prognosis class [24] and offers significant improvements compared to the allogeneic transplant protocol. These improvements are mainly caused by the tumorigenesis within host tissue. The DEN-induced model better replicates the natural TME, preserving native cellular and molecular interactions. This enables a more accurate depiction of tumour-stroma crosstalk, immune responce, and angiogenesis, making it a robust platform for studying cancer development

and progression [25]. DEN-induced tumors arise within the host's own tissue, naturally evading such allogeneic immune recognition. This intrinsic development ensures a more precise and representative model for investigating the dynamic interplay between the tumor and the host's immune system [26].

DEN-induced tumours arise from the host's own cells, undergoing genetic and epigenetic alterations similar to human cancers. This makes the model highly relevant for studying tumorigenesis mechanisms and evaluating targeted therapies, as it accurately replicates the genomic and epigenomic complexity of human malignancies [27]. DEN-induced tumors better reflect human cancer heterogeneity due to their spontaneous emergence within host tissue. This heterogeneity is key for studying tumor evolution and therapy resistance. By mirroring the cellular and molecular diversity of human malignancies, this model aids in developing effective therapies and deepens our understanding of cancer biology [27]. The DEN-induced model closely mimics human cancer progression, making it highly clinically relevant. By replicating tumorigenesis stages, it provides a robust preclinical framework, enhancing the translation of research into effective therapies [25].

However, while DEN alone recapitulates mutagenesis, it lacks the metabolic context of human obesity-driven HCC. To mimic the interplay between steatosis and hepatocarcinogenesis, the DEN-induced mutagenesis is integrated with a non-alcoholic-fatty liver disease (NAFLD) induced by a choline-deficient diet. Steatosis, a hallmark of NAFLD, exacerbates HCC by inducing lipotoxicity, oxidative stress, pro-inflammatory signaling, and immune evasion, creating a tumor-permissive microenvironment [28,29]. By combining DEN's genotoxic effects with diet-induced metabolic stress, this model replicates the transition from steatosis to steatohepatitis, fibrosis, and HCC, while enabling the study of lipid-driven oncogenic pathways (e.g., Hras, Braf) and immunosuppressive mechanisms critical in metabolic syndrome-associated HCC [30].

This system recapitulates the interplay of lipid-driven mitochondrial dysfunction, chronic inflammation, and adaptive immune suppression observed in human NAFLD-HCC, including selective CD4+ T lymphocyte loss, a hallmark of impaired antitumor surveillance [31]. This dual approach provides a clinically relevant platform to evaluate alternative/additional therapies, which target both DEN-induced mutational drivers and steatosis-associated angiogenesis and immune dysfunction [32].

2.7. Warburg effect and pH paradox

The Warburg effect refers to the preference of cancer cells for aerobic glycolysis over oxidative phosphorylation for energy generation, which is a hallmark of cancer. This metabolic shift is important for rapidly dividing cells as it allows for quick ATP production and the generation of essential molecules for growth. The effect is attributed to the regulation of growth factors and hypoxia within the tumor (TME) microenvironment and is proposed to be a normal physiological response to the excess energy demands of fast-multiplying cells. The pH of the TME is affected by the Warburg effect, as cancer cells produce excess lactate, creating acidic extracellular conditions that hinder immune cells and promote tumor growth, spread, and immune suppression [33]. Intracellular alkalosis arises from the activity of pH-regulating proteins, including Na^+-dependent transporters that facilitate the influx of extracellular sodium ions (Na^+) into the cytoplasm. Recent research has demonstrated elevated intracellular sodium concentrations [Na^+]i and intra-tumor osmotic pressure in many tumor tissues compared to adjacent healthy tissues [34,35].

2.8. Monensin's activity as an anti-cancer agent

Monensin is a sodium and proton selective ionophore that increases the permeability of cell membrane to sodium ions [36]. It can conjugate sodium ions (Na^+) into complexes, facilitating sodium transport through the cell membrane due to its high lipophilic properties. It is used as coccidiostat and nonhormonal growth promoter in veterinary practice [37]. Many recent preclinical studies have been demonstrating an antitumoral activity of monensin, in-vitro, in-vivo models and PDX against different tumors. It has been studied on many cancers including neuroblastoma [38], chemo-resistant pancreatic cancer [39], colorectal cancer [40], ovarian cancer [41], prostate cancer [42], and HCC [43]. Yet, its effects on the cell and molecular mechanism are still controversial, and further studies are required to internalize its effects and safety.

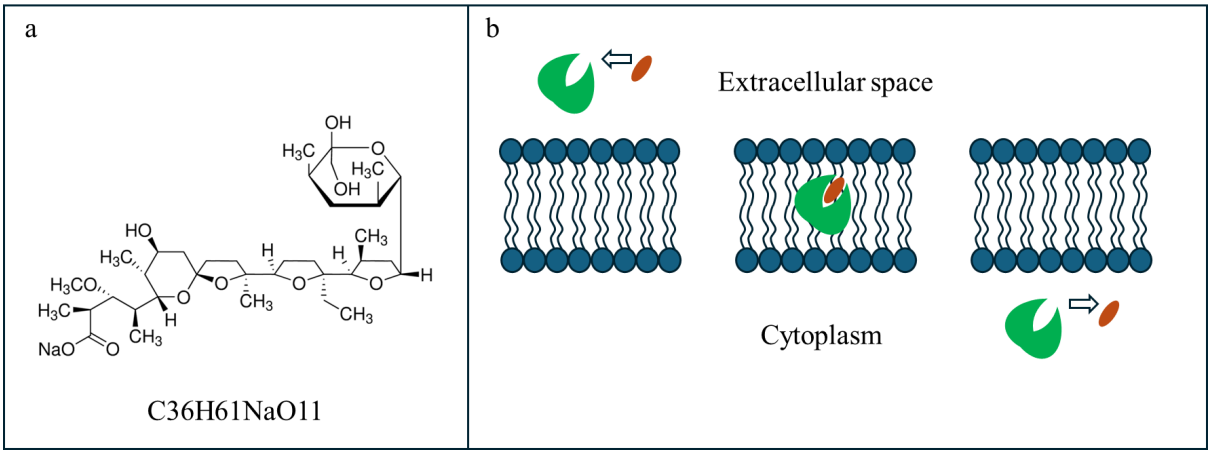

Figure 4: Chemical structure of monensin and its mechanism of action

a: Chemical structure of monensin. b: Mechanism of action of monensin.

Despite previous reports attributing monensin's anticancer effects to its interference with proliferative signalling pathways, recent evidence challenges its classification as a cytostatic agent. In a detailed study on triple-negative breast cancer (TNBC), monensin exhibited **no measurable impact on proliferative markers**, such as Proliferating Cell Nuclear Antigen (PCNA) and Ki-67, in either tumour or healthy proliferative tissues, including the intestine and bone marrow, under physiologically relevant conditions. Rather, the anticancer efficacy of monensin was shown to derive from a **sodium-dependent, tumour-selective cytotoxic mechanism**, which induced cell death without affecting cell proliferation or organ integrity. Notably, monensin-induced reductions in tumour cell density were preceded by intracellular sodium overload and ATP depletion, thereby excluding a direct antiproliferative effect on either malignant or non-transformed cells [44].

In the previous study with an HCC allograft model, we found that HCC cells exhibit an 8–10-fold increase in baseline intracellular sodium $[Na^+]_i$ compared to healthy hepatocytes, as demonstrated via fluorimetry, ICP-MS, and in vivo ^{23}Na-MRI. This imbalance is further exacerbated by monensin, which raises $[Na^+]_i$ by 50–70% specifically in tumour cells ($p < 0.001$), while normal hepatocytes maintain ionic homeostasis. Co-treatment with ouabain, an Na^+/K^+-ATPase inhibitor, intensified monensin's cytotoxicity in HCC cells and sensitised healthy hepatocytes—but only under sodium-replete conditions—highlighting a Na^+-dependent mechanism.

Monensin-induced Na^+ influx initiated a bioenergetic crisis in HCC cells: OxPhos was rapidly impaired, while compensatory glycolysis was transiently activated. ATP levels dropped by 50% within 15 minutes of exposure ($p < 0.001$), leading to energetic collapse. Though glucose supplementation briefly delayed cytotoxicity, sodium-free conditions entirely prevented ATP depletion and cell death. Mitochondrial dysfunction was confirmed by mitochondrial Na^+ accumulation (confocal imaging), membrane hyperpolarisation (2.5-fold increase in JC-1 red/green ratio, $p < 0.01$), and a 40–60% reduction in oxygen consumption rates ($p < 0.01$). Na^+ overload also triggered osmotic stress, evidenced by reduced water efflux (lower kio, $p < 0.001$) and a 30% increase in cell diameter ($p < 0.05$), culminating in necrosis. This was validated by TO-PRO-3 uptake and histology showing a 50% increase in necrotic tumour areas.

In vivo, daily intraperitoneal administration of monensin (8–16 mg/kg) in NSG mice reduced HCC tumour volume by 60–70% ($p < 0.001$), correlating with marked intratumoral Na^+ accumulation (1400 vs. 200 nmol/mg protein, $p < 0.01$). Importantly, monensin spared healthy tissues, with no systemic toxicity, no alteration in organ morphology or weights, and preserved intestinal and bone marrow structure, cellularity, and Ki67 expression [45].

Together, these findings support a **Na^+-driven death cascade** in HCC: sodium overload, ATP depletion, mitochondrial dysfunction, and osmotic swelling converge to induce necrosis. Monensin's **tumour-selective mechanism** and **lack of toxicity in normal tissues** underscore its therapeutic potential for liver cancer [44,45].

3. Objectives of the thesis

This thesis is part of the AIRC-funded project *"Boosting the increase of intracellular sodium to kill selectively hepatic cancer cells: preclinical proof of concept"*, which aims to develop targeted therapies for HCC. Prior work from this project demonstrated that monensin, a sodium ionophore, induces mitochondrial dysfunction and selective cancer cell death in HCC models in vitro and in ectopic in vivo settings, without exhibiting toxicity to normal tissues. Importantly, it was previously suggested—and here further validated—that monensin does not act through direct antiproliferative effects on healthy cells; instead, the observed reduction in tumour cell proliferation is primarily due to cell death induction, confirming its selectivity.

This study builds upon these findings by investigating monensin's efficacy in a translationally relevant, immunocompetent model of NAFLD-associated HCC, induced through DEN administration [46,47] and a choline-deficient, L-amino acid-defined (CDAA) diet [31]. This model closely replicates the progression of human NAFLD-HCC, encompassing steatosis, inflammation, metabolic dysregulation, immune alterations, and tumour development, while preserving an intact tumour-immune microenvironment.

Our objective is to imvestigate monensin's effects on reducing tumour burden, interfering with lipid-driven oncogenic signalling, and modulating immune responses in vivo. By bridging previous mechanistic insights with a physiologically and immunologically relevant setting, this study provides preclinical evidence for monensin as a selective, dual-acting therapeutic agent targeting both metabolic and immune pathways in NAFLD-driven HCC.

4. Materials and methods

4.1. Chemicals and reagents

Fetal Bovine Serum (FBS), Bovine Serum Albumin (BSA), penicillin (P), streptomycin (S), monensin, (2-Hydroxypropyl)-β-cyclodextrin (HPβCD), Na+ pyruvate (Na+ Pyr), and all chemicals used for buffers and reagents preparation were sourced from Sigma-Aldrich (Milan, Italy). Dulbecco's Modified Eagle Medium (DMEM), and a custom-modified sodium-free DMEM (DMEM-Na+), lacking any sodium components, Glutamax 1000, and MEM Non-Essential Amino Acids (NEAA) were procured from GIBCO (S.I.A.L. group, Rome, Italy). BCA Protein assay kit and Clarity ECL Western Blotting Substrate were purchased from Thermo Fisher Scientific (Waltham, Massachusetts, USA).

4.2. Experimental animals and in vivo investigation

Male C57BL/6 neonatal mice, with an initial body weight ranging from 5 to 6 grams, were intraperitoneally (i.p.) administered a single DEN dose of 0.021 μL per gram of body weight. The administration of DEN served as an initiating step to induce hepatocarcinogenesis. Following the weaning period, which typically occurs within the third to fourth week of life, the animals were transferred to and maintained under controlled laboratory conditions on a specialized CDAA diet. This diet was formulated to facilitate the induction and progression of pathological changes in the liver, specifically aiming to promote hepatic steatosis, chronic inflammation, fibrosis, and eventually the development of HCC. These conditions collectively establish a robust experimental model for studying liver disease pathogenesis and the molecular mechanisms underlying hepatocarcinogenesis. The animals were maintained in the animal facility of the Health Sciences Department of Università del Piemonte Orientale, and treated in accordance with the University Ethical Committee and European guidelines (Experimental protocol authorization n. 851/2020-PR, released on 19/08/2020 from Italian Ministry of Health for protocol n.DB064.60).

4.2.1. Animal treatment protocol

Upon completion of a 20-week period during which the mice were maintained on the CDAA diet, we initiated a six-week treatment regimen. This consisted of daily i.p. administration of monensin at a dosage of 8 mg/kg body weight or an appropriate vehicle control. The therapeutic intervention was aimed at evaluating the potential efficacy and safety of monensin in mitigating liver pathology and disease progression. At the conclusion of the treatment period, the animals were euthanized under ethical and controlled conditions, in compliance with laboratory animal care protocols. Subsequently, the livers, along with any nodular formations indicative of neoplastic changes, were meticulously harvested and preserved for comprehensive histopathological evaluation. Throughout the treatment, the body weight of the mice was monitored routinely as a surrogate marker to assess both the safety profile of the administered compound and its impact on the overall health of the subjects.

4.2.2. Quantitative analysis of cell density

Tumour cell density was assessed using haematoxylin and eosin (H&E) staining of paraffin-embedded tissue sections obtained from 25 mice (13 treated with monensin vs 12 control). Excised tumour nodules were fixed in 10% neutral-buffered formalin for 24 hours, dehydrated through a graded ethanol series, and embedded in paraffin. Sections of 4 µm thickness were obtained using a microtome and mounted on glass slides. After deparaffinization and rehydration, the slides were stained with haematoxylin to visualise cell nuclei and eosin to highlight the cytoplasm and extracellular matrix. High-definition (0.17 um/px) images were captured using a Zeiss Axioscan 7 slide scanner under high-power fields (HPFs, 400× magnification). Tumor cell densities (cells/mm²) over the entire slides were quantified using the quantitative pathology analysis software QuPath 0.5.1 through the built-in cell-detection analysis. Data were analysed statistically to compare variations in cellularity between experimental groups.

4.2.3. Quantitative analysis of CD31+

To evaluate intratumoral angiogenesis, immunohistochemical staining for CD31 (platelet endothelial cell adhesion molecule-1, PECAM-1) was performed on formalin-fixed, paraffin-embedded liver sections from 25 mice (13 treated with monensin vs 12 control). Tissue sections (4 μm) were deparaffinized, rehydrated, and subjected to heat-induced antigen retrieval using citrate buffer (pH 6.0). Endogenous peroxidase activity was blocked with 3% hydrogen peroxide, followed by incubation with a rabbit anti-CD31 monoclonal antibody (clone D8V9E, Cell Signaling Technology, 1:100 dilution) overnight at 4°C. Detection was achieved using a horseradish peroxidase (HRP)-conjugated secondary antibody and 3,3′-diaminobenzidine (DAB) chromogen, with hematoxylin counterstaining. CD31-positive microvessels were quantified over the entire section through the quantitative pathology analysis software QuPath 0.5.1 through the built-in positive-cell-detection function. Statistical analysis was performed using Student's t-test to compare mean microvessel density (MVD) between groups. This approach aligns with established methodologies for evaluating anti-angiogenic therapies in preclinical HCC models [48].

4.2.4. Quantitative analysis analysis of CD8+

The quantification of CD8+ T cells in tumour sections from 25 mice (13 treated with monensin vs 12 control) was executed over the entire section through the quantitative pathology analysis software QuPath 0.5.1 through the built-in positive-cell-detection function. Hematoxylin optical density (OD) was selected as the detection parameter, with a requested pixel size of 0.5 μm to ensure high-resolution analysis. Nucleus segmentation was optimised using a background radius of 5 μm, sigma value of 0.75, and a minimum nucleus area threshold of 9 μm² to exclude non-cellular artifacts. Intensity-based thresholding was applied with a set value of 0.05, and shape-based splitting was enabled to improve the accuracy of cell separation and smooth boundary detection was enabled to enhance measurement accuracy. This automated approach allowed for precise quantification of CD8+ T cell infiltration within tumour tissues, providing valuable insights into the immune response in the tumour microenvironment.

4.2.5. Quantitative analysis of Steatosis

Monensin effects on hepatic lipid accumulation and neoplastic progression was evaluated. Steatotic changes were assessed through histopathological analysis of liver sections stained with H&E. Comparative evaluation of lipid droplet distribution, hepatocellular ballooning, and inflammation was performed between control and monensin-treated groups using QuPath 0.5.1. Quantitative metrics, including steatosis grade (percentage of lipid vacuoles distribution/mm^2) and necroinflammatory activity, were derived by analyzing the entire slides. All protocols adhered to institutional ethical guidelines for animal research.

4.2.6. Quantitative RT-PCR (qPCR) analysis of inflammatory biomarkers

Total RNA was extracted from fresh tumor tissues using TRIzol Reagent (Invitrogen) according to the manufacturer's instructions. RNA concentration and purity were assessed spectrophotometrically using a NanoDrop™ instrument (Thermo Fisher Scientific). Reverse transcription was performed using High-Capacity cDNA Reverse Transcription Kit (Applied Biosystems Italia, Monza, Italy), with 2 µg of RNA converted into complementary DNA (cDNA) following the recommended protocol in a Techne TC-312 thermocycler (TecneInc, Burlington NJ, USA). The resulting cDNA was amplified by PCR using gene-specific primers and Master mix Fast Start SYBR Green (Roche). Amplifications were carried out in a CFX96™ Real-time PCR System (Bio-Rad, Hercules, California, USA). Gene expression levels were normalised to β-actin, and relative quantification was calculated using the ΔΔCt method.

4.3. Cell culture and in vitro investigation

Murine C1C7 HCC cells were supplied by ECACC (Salisbury, UK). C1C7 cells were routinely cultured in DMEM, supplemented with 10% FBS, 100 U/mL P, 100 µg/ml S, 6 mM Gln, 1 mM Na+ pyruvate (Na+ Pyr) and 1% MEM-NEAA. Cells were maintained in a humidified chamber at 5% CO2 / 95% air at 37 °C and split every 1 to 3 days. All cells tested negative for mycoplasma with Mycoplasma PCR Detection Kit (Abcam, Inc.).

4.3.1. Analysis of the sodium-dependent cytotoxic effect of monensin

C1C7 cells were seeded at 10,000 cells per well in 96-well plates, in triplicate, and incubated for 24 hours to form a uniform monolayer. For sodium measurements, cells were loaded with 5 µM CoroNa Green dye—a sodium-specific fluorescent indicator that increases green fluorescence intensity upon Na^+ binding, without shifting its emission wavelength—for 30 minutes at 37 °C in a humidified atmosphere of 5 % CO_2. Following incubation, two washes with serum-free DMEM were performed to remove residual dye and avoid esterase inhibition by serum components.

Sodium-Dependent Cytotoxicity: after CoroNa Green loading, cells received were treated with monensin (5 µM) or its vehicle DMSO (control) in either standard sodium medium (DMEM containing 145 mM Na^+) or sodium-free medium (DMEM without any Na^+). Concurrently, **0.6**µM IncuCyte® Cytotox NIR Dye (a DNA-binding probe that fluoresces upon cell-membrane compromise) was added to enable real-time necrosis monitoring.

Real-time imaging was performed on an automated widefield live-cell system (IncuCyte SX5 Live Cell Analysis System, Sartorius®), which employs predefined (preset) acquisition settings for optimal signal fidelity (accuracy and reliability). Brightfield and multi-channel fluorescence images were captured with a 20× objective. The following excitation/emission configurations were utilised: CoroNa Green: 492 nm ex / 516 nm em, Cytotox NIR Dye: 491 nm ex / 509 nm em.

To ensure uniformity (consistency) across all experimental conditions, identical LED intensities, exposure times and focus offsets were applied. Quantitative image data—fluorescence intensities and cell counts—were automatically extracted by the IncuCyte software and exported as comma-separated values (.CSV) for subsequent statistical analysis.

4.3.2. Quantitative analysis of proliferation biomarker

Following each treatment regimen with palmitic acid (PA) and monensin, cells were washed twice in ice-cold PBS and lysed in RIPA buffer (Thermo Fisher Scientific) supplemented with protease and phosphatase inhibitors (Sigma-Aldrich).

Protein concentration was determined by BCA assay (Thermo Fisher Scientific), and 10–20 µg of total protein per sample were placed on 10% polyacrylamide gels. Proteins were transferred onto Amersham™ Hybond® P PVDF membranes (Cytiva) using a dry-transfer apparatus. Membranes were blocked for 1 hour at room temperature in 10% bovine serum albumin (BSA) in TBS-T (0.1% Tween-20) before overnight incubation at 4 °C with primary antibodies against PCNA (Sigma-Aldrich (MO, USA) and β-actin (Sigma-Aldrich (MO, USA). After washes in TBS-T, blots were incubated with species-specific HRP-conjugated secondary antibodies for 1 hour at room temperature. Signals were detected by enhanced chemiluminescence (ECL; Thermo Fisher Scientific) and imaged on a ChemiDoc MP system (Bio-Rad). Band intensities were quantified in ImageJ and normalised to β-actin, permitting direct comparison of proliferative markers expression across both untreated and PA-pretreated conditions.

4.3.3. Intracellular lipid accumulation

We used HCS LipidTOX™ Phospholipidosis and Steatosis Detection Kits (Invitrogen) to assess intracellular steatosis. Cells were plated as a monolayer in 96 well plates at 2000 cells per well, in triplicate, for 24 hours, This was followed by 24 hours of pretreatment with PA 25µM or vehicle, washed with PBS, and replaced with 24 hours treatment with monensin 5µM, PA 25µM, or vehicle. Cells were fixed with paraformaldehyde (PFA) 4% for 10 minutes and permeabilized with PBS 1X Tryton 0.1% for 20 minutes, then washed with PBS. Subsequently, Steatosis Detection Kit was added at 1:1000 dilution for 30 minutes, followed by DAPI staining 1% for 10 minutes. The EVOS® FL Auto Imaging System was used to read the plate, and images were ImageA as a percent of the intracellular lipid droplet area to the area of cells.

4.3.4. PA effects on monensin cytotoxicity

To assess whether PA affects monensin-induced cell death, we used Trypan Blue (TB) exclusion assay to determine viability assay based on membrane integrity. 10,000 C1C7 cells per well were plated in a 24-well plate for 24 hours to form a uniform monolayer. This was followed by 24 hours of pretreatment with PA 25µM or vehicle, washed with PBS, and replaced with 24 hours treatment with monensin 5µM, PA 25µM, or vehicle. We collected the

supernatant into 2ml eppendorf, then detached the cells with 150µL of trypsin, that was inhibited by 300µM of media, all added to the same eppendorf, centrifuged and suspended in proper volume of media to have countable cell density.

4.4. Statistical analysis

All in vitro experiments were conducted independently at least three times, data are expressed as the mean ± standard deviation from three to five independent experiments. Statistical significance between two groups was assessed using an unpaired or paired two-tailed Student's *t*-test. For comparisons involving multiple groups or time-course analyses, one-way ANOVA and two-way ANOVA were applied, respectively. The normality of data distribution was verified in advance using the Kolmogorov-Smirnov test. A significance threshold of 5% was set, with $P < 0.05$ considered statistically significant ($P < 0.05$, $*P < 0.01$, $**P < 0.001$). Statistical analyses were performed using GraphPad Prism v.8.4.3 (GraphPad Software, San Diego, CA, USA).

5. Results

5.1. Quantitative analysis of HCC nodules

Optical evaluation of livers demonstrated a significant reduction in both the number and volume of HCC nodules in the treated group compared to the control group (Fig. 5). The nodules in the treated group appeared smaller, and more discrete, indicating a potential therapeutic effect in limiting tumour progression and growth. These findings suggest that the

administered treatment may have effectively suppressed hepatocarcinogenesis and mitigated tumour burden, as evidenced by the optical morphological assessment. The statistical analysis was performed using Mann-Whitney test.

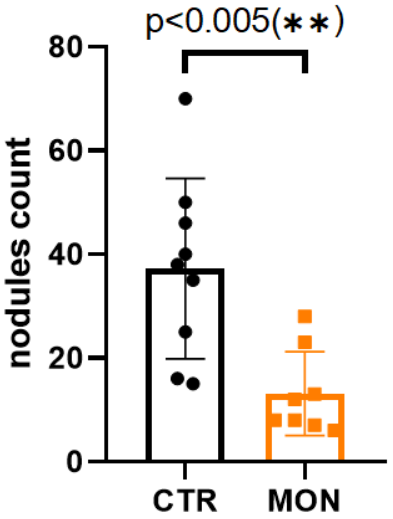

Figure 5: Quantitative analysis between the nodules number in liver from control and treated groups.

5.2. Quantitative analysis of cells density

HCC nodule decrease (both as size and number) was associated with an extended tumor damage and necrosis, as demonstrated by histological observations (Fig. 6 a, b), and measured by a decrease of the cellular density (Fig. 6c). This reduction in cellular density aligns with prior evidence that monensin induces necrotic cell death in HCC cells via Na^+ overload, osmotic stress, and mitochondrial dysfunction—a mechanism amplified in cells with defective ion regulation [45].

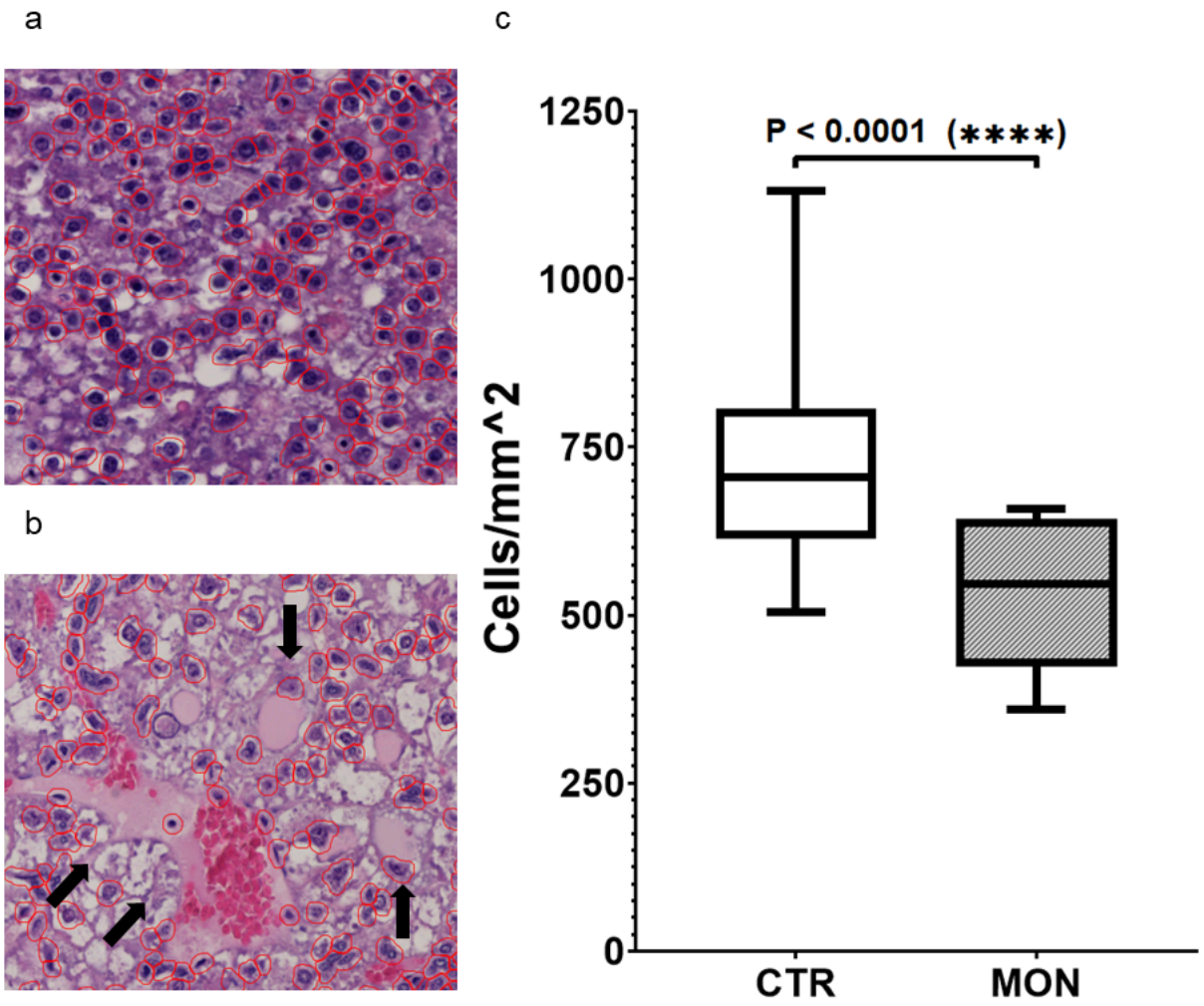

Figure 6: (H&E) stained histological section from HCC nodules obtained from control and treated mice. Representative H&E images of HCC nodule section of mice i.p. treated with vehicle a) or Monensin. Necrotic areas are indicated by black arrows. c) Quantification of tumor cellular density evaluated as cells/mm2 in vehicle (CTR) or Monensin treated mice. Bars represent the average while error bars represent the standard deviation. ****P < 0.0001 by unpaired T test.

The statistical significance of these findings (Fig. 6c) supports monensin's potential as a therapeutic agent for HCC and suggests that intervention during carcinogenic progression may halt or delay tumorigenesis.

5.3. Quantitative analysis of CD31+

The density of CD31+ cells was significantly reduced in hepatic tissues of mice treated with monensin (Fig. 7b) compared to control groups (Fig. 7a). This reduction was associated with the decreased number of hepatic nodules and with their smaller dimensions.

Immunohistochemical analysis across liver sections from DEN-induced carcinogenesis cohorts quantified a marked decline in CD31+ cells in monensin-treated mice. Furthermore, this was confirmed also by RT-qPCR assessing the expression in the tumor samples (Fig. 7c). Automated positive-cell counting further substantiated this observation, revealing a significant decrease in the percentage of CD31+ cells in treated groups (Fig. 7d).

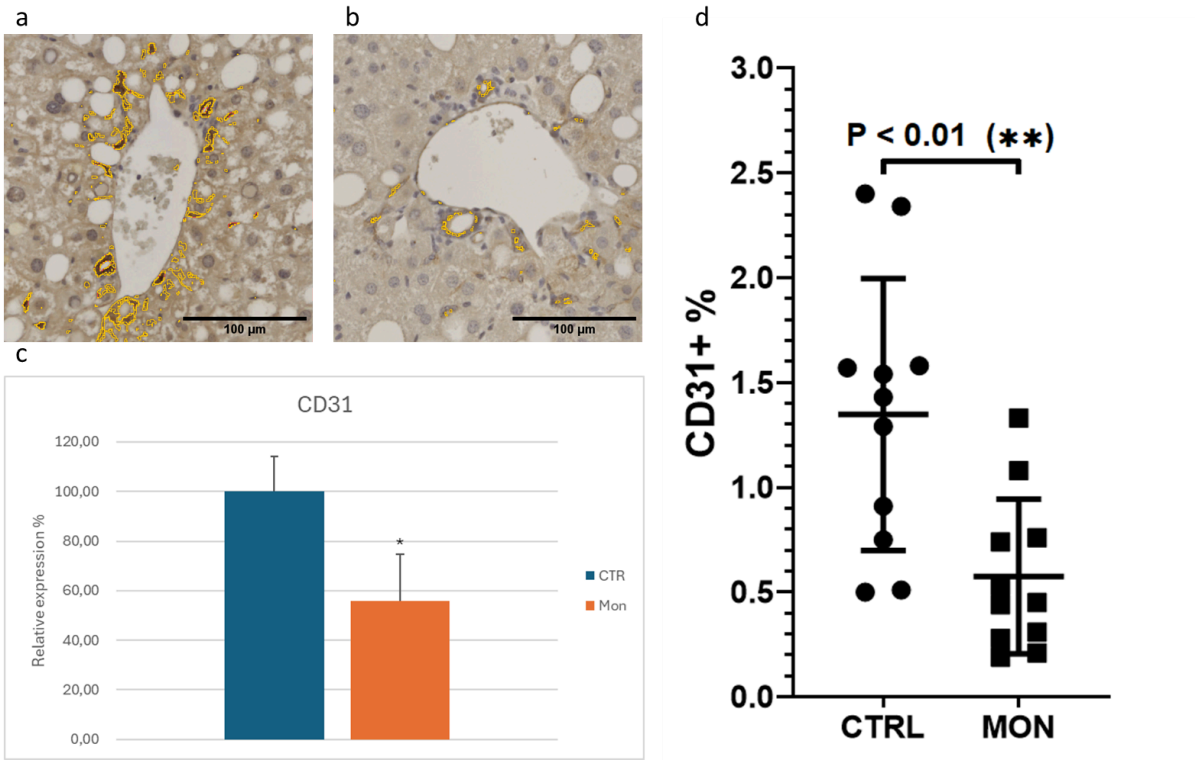

Figure 7: Immunohistochemical analysis of CD31+ in livers obtained from control and treated mice.

a: Control group. b: Monensin group. c: RT-qPCR quantification of CD31 in HCC nodules from livers of control and monensin treated mice. d: CD31+ quantification (percentage of positive CD31 to the total cell count) of liver sections of control and monensin treated mice. Bars represent the average while error bars represent the standard deviation. **P < 0.01 by unpaired T test.

Collectively, these findings suggest that monensin exerts dual antitumor effects: it directly induces cytotoxicity in HCC cells while exerting anti-angiogenic properties. By inhibiting the formation of new blood vessels, monensin might, in fact, effectively constrain neoplastic progression.

5.4. Quantitative analysis of CD8+

The immunohistochemical analysis revealed a significant increase in CD8+ cytotoxic T-cell density within hepatic tissues of monensin-treated mice (Fig. 8b) compared to controls (Fig. 8a), as quantified across entire liver sections from DEN-induced carcinogenesis cohorts. Automated cell counting demonstrated an elevation in CD8+ cell density in treated groups that was parallel with a reduction in both the number and size of hepatic nodules. This inverse relationship suggests that monensin not only exerts direct cytotoxic effects on HCC cells but also enhances antitumor immunity by promoting CD8+ T-cell infiltration, thereby possibly further inhibiting neoplastic progression. Notably, the statistical robustness of these results (e.g., monensin cohorts averaged ~98,58 CD8+/mm² vs. control ~61,31 CD8+/mm²) reinforces the reproducibility of monensin's immunomodulatory effects.

The observed increase in CD8+ T-cell density aligns with monensin's previously reported mechanism of Na^+-mediated necrotic cell death. Necrotic tumor cells release damage-associated molecular patterns (DAMPs) and tumor antigens, which may stimulate dendritic cell activation and subsequent priming of CD8+ T-cells. This immunogenic cell death mechanism could explain the heightened immune surveillance in treated mice, as cytotoxic T-lymphocytes are recruited to eliminate residual cancer cells. Furthermore, the smaller nodule dimensions and reduced tumor burden in monensin-treated cohorts suggest that CD8+ T-cells might play a critical role in suppressing tumor growth, potentially through direct lysis of malignant cells.

These findings are consistent with prior studies highlighting monensin's tumor-selective action and absence of systemic toxicity [43,44]. The enhanced CD8+ infiltration, coupled with reduced nodularity, underscores the dual therapeutic potential of monensin: it directly disrupts cancer cell viability via ion dysregulation while indirectly mobilizing the adaptive immune system to target residual lesions.

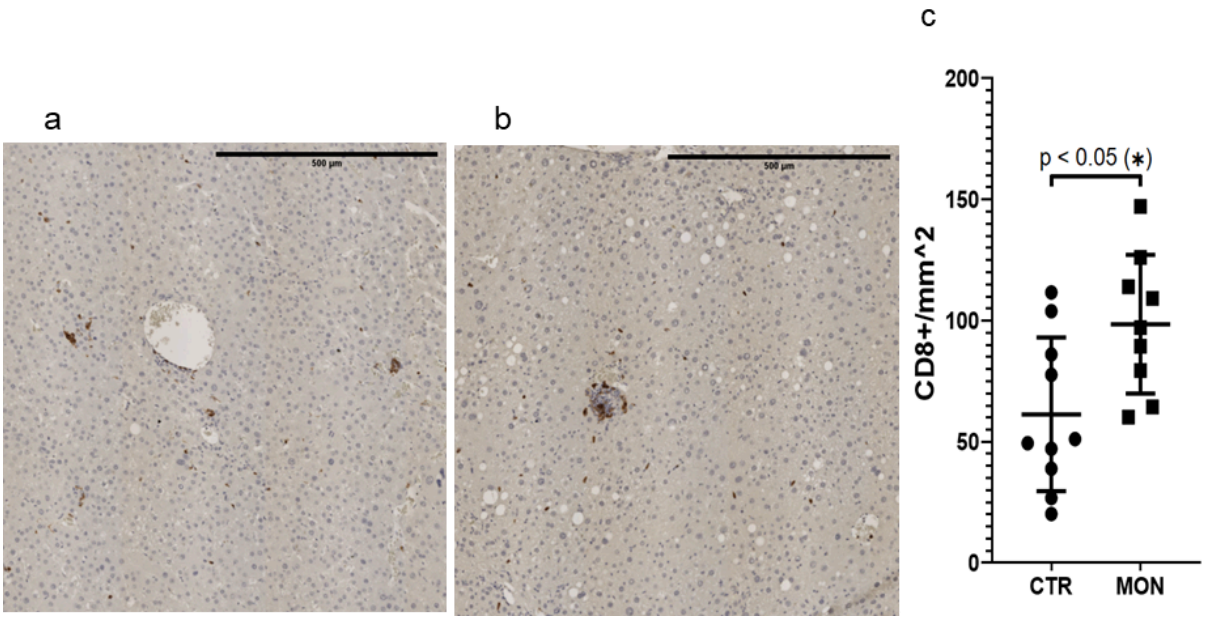

Figure 8: Immunohistochemical analysis of CD8+ in livers obtained from control and treated mice.

a: Control group. b: Monensin group. c: Quantification of CD8+ lymphocytes in liver sections of control and monensin treated mice. Bars represent the average while error bars represent the standard deviation. *P < 0.05 by unpaired T test.

5.5. Quantitative analysis of steatosis

Histopathological analysis revealed a significant reduction in hepatic steatosis in monensin-treated mice (Fig. 9c,d) compared to controls (Fig. 9a,b), as evidenced by decreased lipid droplet accumulation. Control cohorts exhibited widespread macrovesicular steatosis (19% of hepatocytes affected), whereas monensin-treated livers showed 5% less lipid-laden cells ($p < 0.05$), correlating with diminished hepatocellular ballooning and lobular inflammation. This attenuation of steatosis was associated with prior observations of monensin-induced tumor regression and CD8+ T-cell infiltration, suggesting a multifactorial therapeutic mechanism. The reduction in lipid accumulation may reflect monensin's disruption of Na^+-dependent metabolic pathways, as its ionophoric activity has been shown to impair ATP production[43] thus possibly affecting lipid synthesis and transport in malignant hepatocytes.

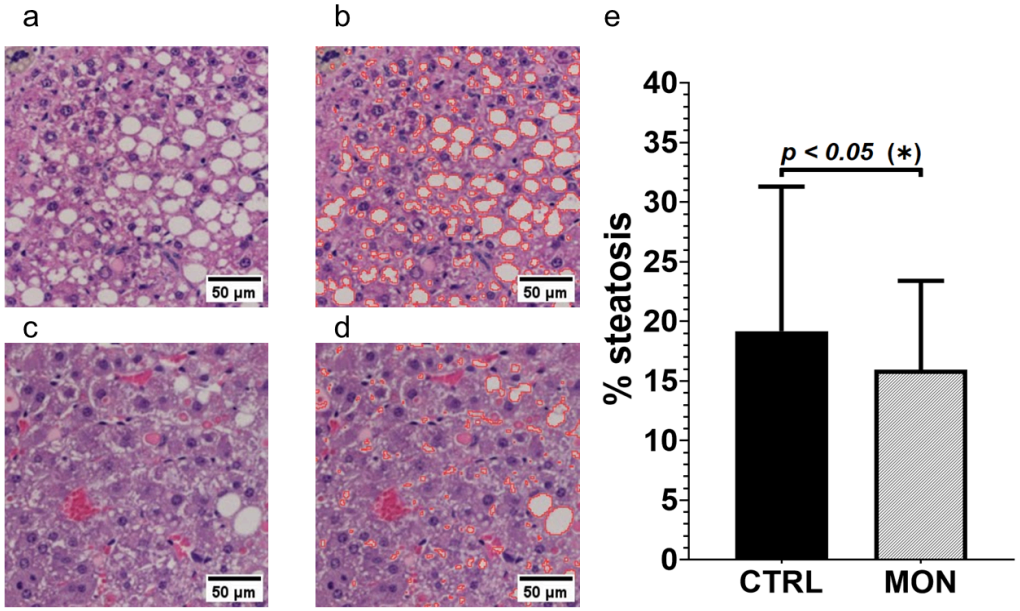

Figure 9: Steatosis histopathological analysis of liver sections obtained from control and treated mice.

a, b: Sections from the control group. c, d: Sections from the monensin group. e: Steatosis quantification in HCC nodules from liver of control and monensin treated mice. Bars represent the average while error bars represent the standard deviation. *P < 0.05 by unpaired T test.

5.6. Quantitative RT-PCR (qPCR) analysis of inflammatory biomarkers

QPCR analysis revealed elevated proinflammatory markers in tumors belonging to monensin-treated mice, such as IL1, IL6 Tumor necrosis factor a (TNFa), interferon gamma (INFg), and elevated M1 macrophages, with no effects on anti-inflammatory markers or on M2 macrophages. These findings with the elevated CD8+ infiltration, represent a proinflammatory effect in the tumor induced by monensin, which results in immune cells recruitment to the tumor, rendering it more visible for the immune system.

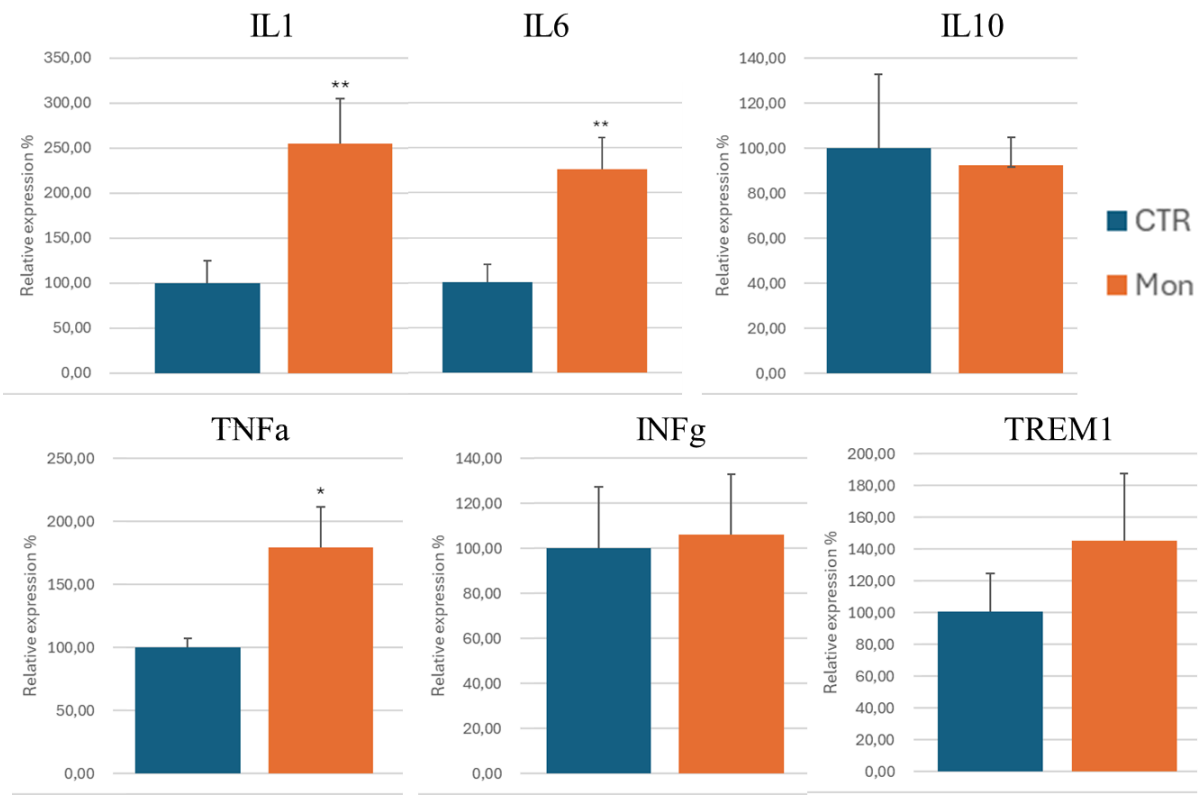

Figure 10: Inflammatory markers levels in tumors obtained from control and monensin treated mice. RT-qPCR quantification of IL1, IL6, IL10, TNFa, INFg, and TREM1 in HCC nodules from livers of control and monensin treated mice. Bars represent the average while error bars represent the standard deviation. *P < 0.05, **P<0.005 by unpaired T test.

5.7. Sodium-dependent cytotoxicity of monensin

The anti-cancer activity of Monensin on HCC cells was assessed by cytotoxicity in vitro assays. C1C7 cells were plated with DMEM ± Na^+ and treated with Monensin 5μM or vehicle. The results showed that Monensin reduced the HCC cells viability starting from the 13th hour of treatment only in presence of extracellular sodium (Fig. 11).

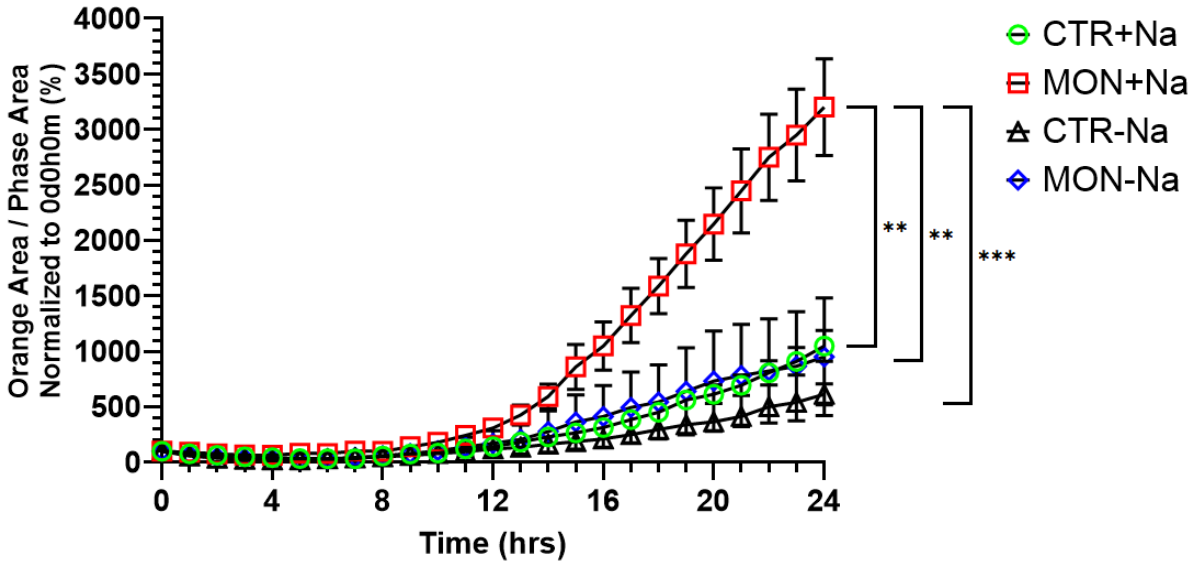

Figure 11: Effect of Monensin on C1C7 cells in different media. Cytotoxic effects of 24 hours of treatment with 5µM Monensin on C1C7 cells.

The grouped superimposed plot shows the positivity to propidium iodide in DMEM±Na+. **P < 0.005, ***P<0.0005 by ordinary one way ANOVA.

5.8. Quantitative analysis of proliferative biomarker

To assess whether monensin modulate proliferative markers expression, in presence or absence of Palmitic Acid (PA), we performed two independent Western blot series in C1C7 cells: one with a 48 h PA pretreatment, followed by 24 h of monensin, and one without any PA pretreatment. C1C7 cells were seeded in 6-well plates and processed in two parallel Western blot workflows. In the **first series**, cells received no PA pretreatment and were exposed for 24 hours to monensin (5 µM), PA (10 µM or 25 µM), or their combination, alongside vehicle controls. In the **second series**, cells were preincubated with PA (10 µM or 25 µM) for 48 hours prior to 24-hour treatments.

Densitometric analysis of Western blots for PCNA (DNA synthesis marker) normalised to β-actin revealed minimal variation across cells treated with monensin or PA or thier controls for 24 hours. Similarly, The stability of PCNA levels across the different conditions of monensin and PA treatments indicates that monensin does not exert a detectable antiproliferative on C1C7 cells under these conditions. These observations support our

hypothesis that any reduction in viable cell number is attributable to a selective cytotoxic mechanism rather than non-specific inhibition of proliferation. This finding aligns with prior in vitro and in vivo studies, which likewise showed preserved proliferative indexes in surviving cells despite substantial tumour shrinkage [44,45].

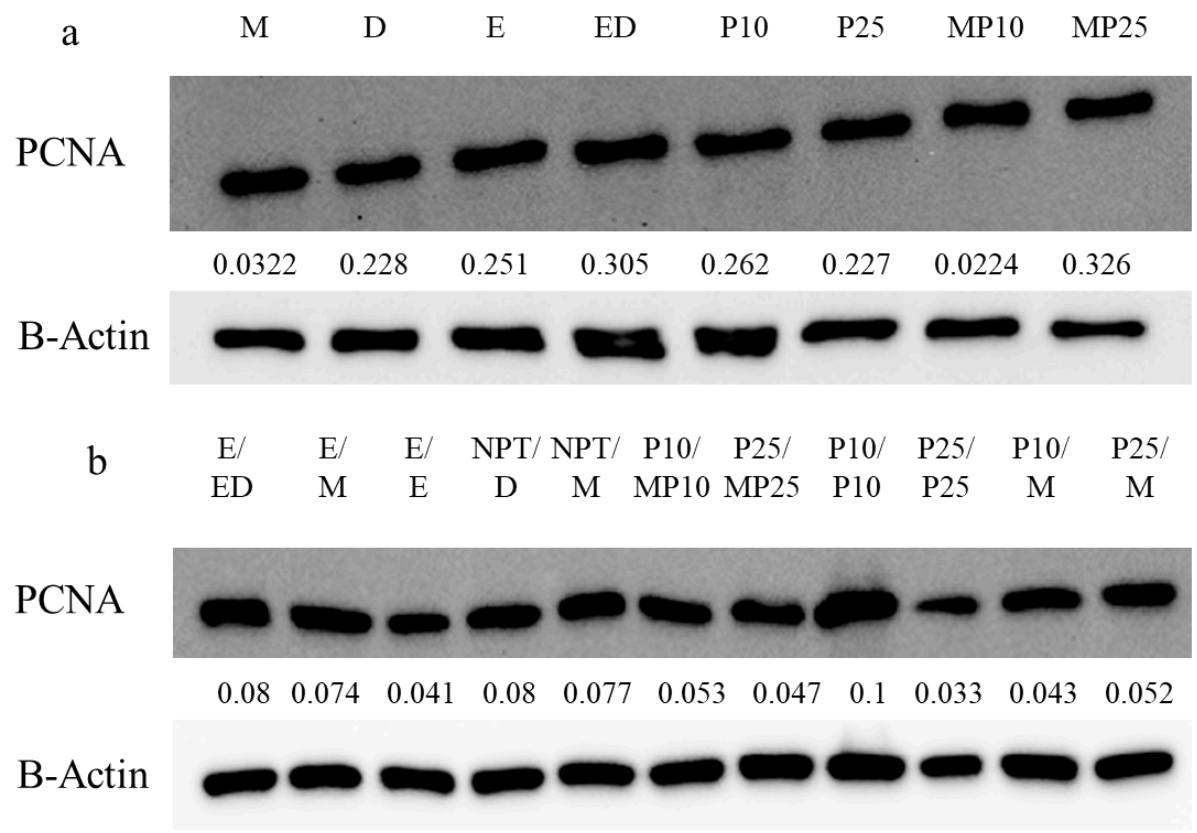

Figure 12: Effect of monensin on the expression of the proliferative marker PCNA in steatotic C1C7 cells. Western blot analysis and densitometric quantifications showing actin-normalized PCNA protein levels of a: Treated cells with combinations of monensins and Palmitic Acid (PA) and the proper controls. b: Pretreatment with PA (first row) and treatment with combinations of monensins and PA and the proper controls (second row). M: Monensin 5µM. D: DMSO 5µM. E: Ethanol 25µM. ED: Ethanol 25µM plus DMSO 5µM. P10: PA 10 µM. P25: PA 25µM. MP10: Monensin 5µM plus PA 10 µM. MP25: Monensin 5µM plus PA 25µM. NPT: No pretreatment. NT: No treatment. Data represent a typical experiment of 3.

5.9. Evaluation of monensin effect on intracellular lipid accumulation

We preliminarily evaluated the effect of monensin treatment on intracellular lipid accumulation of HCC cells using the **EVOS® FLAuto Imaging System**. Cells that were pretreated with 25µM Palmitic Acid (PA) for 24 hours then treated with 25µM of PA for another 24 hours (P25/P25) showed increased volumes and higher number of intracellular lipid droplets

(Fig. 13a). When monensin was added to the treatment (P25/MP25), we noticed a reduction in the volume and number of the lipid droplets.

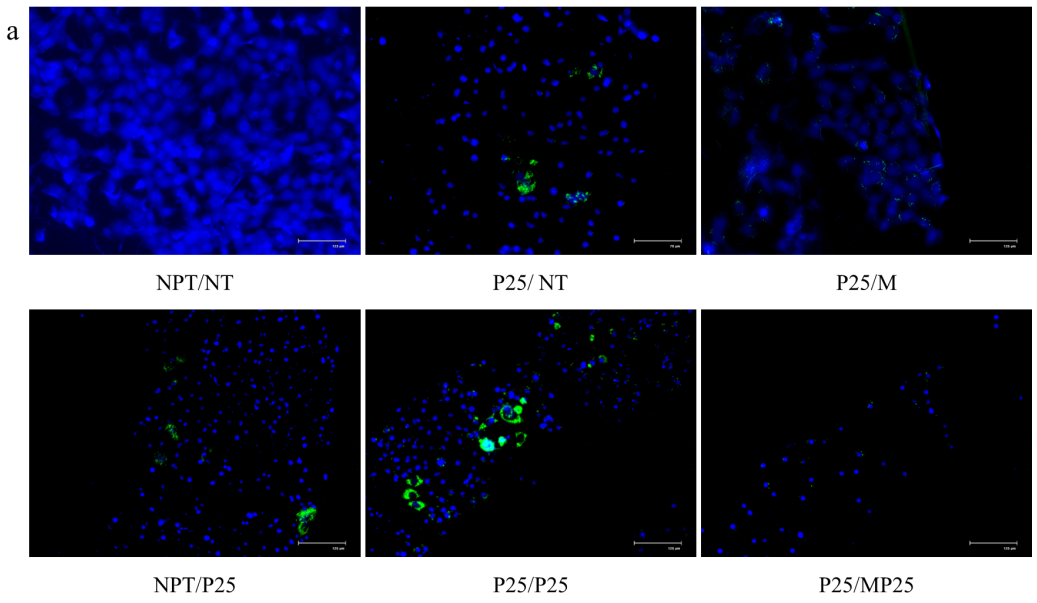

Figure 13: Intracellular lipid accumulation analysis by EVOS® FL Auto Imaging System using Steatosis Detection Kit and DAPI staining.

a: Images captured of cells incubated with PA with or without monensin treatment. M: Monensin 5µM. D: DMSO 5µM. E: Ethanol 25µM. ED: Ethanol 25µM plus DMSO 5µM. P10: PA 10 µM. P25: PA 25µM. MP10: Monensin 5µM plus PA 10 µM. MP25: Monensin 5µM plus PA 25µM. NPT: No pretreatment. NT: No treatment.

5.10. Palmitic acid (PA) effects of monensin cytotoxicity

To assess whether Palmitic Acid (PA) affects monensin-induced cell death, we used Trypan Blue (TB) exclusion assay to determine cell viability. We performed a 24 hours of pretreatment with PA 25µM or vehicle, followed by 24 hours treatment with monensin 5µM (P25/M), PA 25µM (P25/P25), their combination (P25/MP25). As control for P25/P25, we incubated the cell with 25µM of ethanol for 48 hours (E/E), or for 24 hours followed by 24 hours with monensin (E/M) as control for P25/M. There was no statistically significant difference between most of the paired comparisons (except when comparing monensin treated and non-treated cells), including P25/MP25 vs E/M, both in 16 hours and 24 hours. These results indicate that PA does not affect monensin cytotoxicity, which is translated into the retention of monensin activity in steatotic liver conditions.

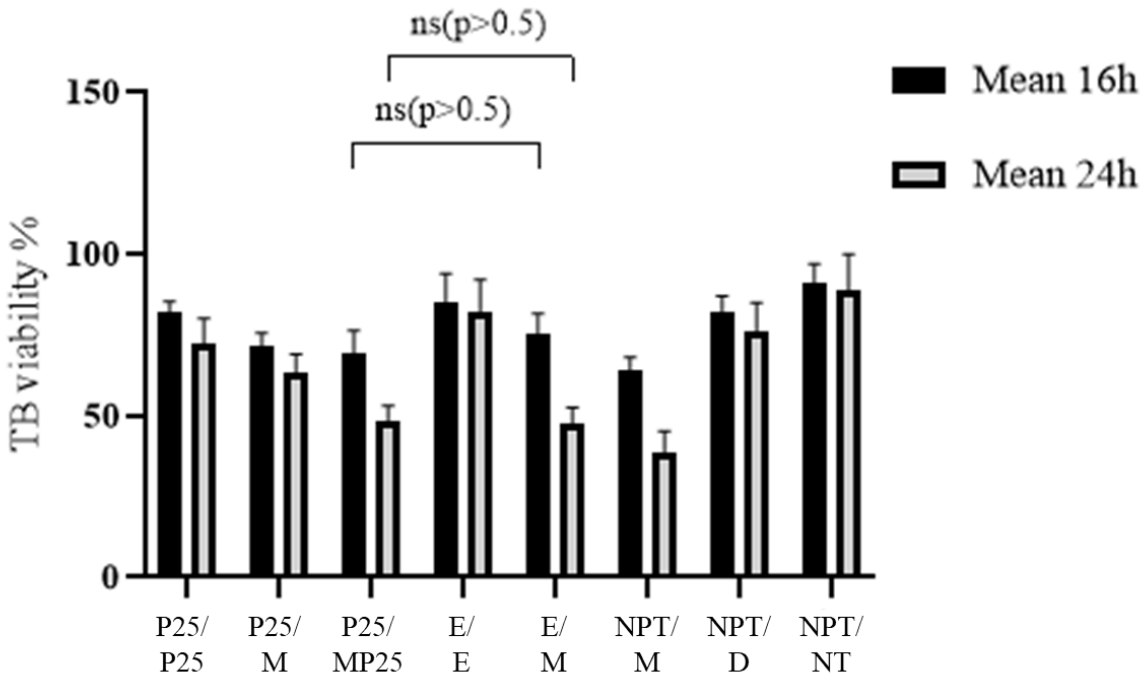

Figure 14: Statistical analysis of TB based exclusion assay using Two way ANOVA with Tukey's multiple comparisons test.

First row: Pretreatment with PA. Second row: Treatment with combinations of monensins and PA and the proper controls. M: Monensin 5µM. D: DMSO 5µM. E: Ethanol 25µM. ED: Ethanol 25µM plus DMSO 5µM. P25: PA 25µM. MP25: Monensin 5µM plus PA 25µM. NPT: No pretreatment. NT: No treatment. By two way ANOVA multiple comparison.

6. Discussion

The present thesis demonstrates that monensin treatment exerts potent antitumor effects in a highly translational relevant murine model of NAFLD-DEN induced HCC, as evidenced by significant reductions in both the number and size of hepatic nodules. These morphological changes were accompanied by a significant decrease in tumor vascularization (CD31+) and steatosis, along with a marked increase in CD8+ T-cell infiltration within the tumor microenvironment. Together, these findings suggest that monensin targets HCC through a multifaceted mechanism involving direct tumor cell cytotoxicity, anti-angiogenic effects, metabolic reprogramming, and immune modulation.

The reduction in tumor nodules aligns with monensin's established ability to disrupt intracellular Na+ homeostasis, leading to ATP depletion, mitochondrial dysfunction, and necrotic cell death. Notably, the decreased vascularization (CD31+) in treated tumors may reflect either an anti-angiogenic effect of monensin or secondary vascular collapse following tumor cell death. This is particularly relevant in HCC, where angiogenesis is a hallmark of progression. The concurrent reduction in steatosis suggests that monensin may additionally interfere with lipid metabolism in malignant hepatocytes, potentially through its effects on Na+-dependent metabolic pathways.

Perhaps most intriguing is the observed increase in tumor-infiltrating CD8+ T-cells following monensin treatment, and the elevated proinflammatory markers such as inflammatory interleukins and M1 macrophages. This immunomodulatory effect could result from several mechanisms. The most logical one can be attributed to the released tumor antigens from the necrotic tumor cell death, in parallel with increased secretion of proinflammatory proteins, which stimulate immune cells recruitment and dendritic cell activation and T-cell priming. Other mechanisms can result from monensin effects on the tumor microenvironment that reduces immunosuppressive signals, or enhanced T-cell trafficking due to vascular normalization. The combination of reduced tumor burden and enhanced immune infiltration suggests that monensin may create a more immunogenic tumor microenvironment, potentially sensitizing HCC to checkpoint immunotherapy.

Additionally, monensin reduced steatosis in vivo in the DEN-NAFLD induced HCC, while in vitro revealed no effect of PA on monensin activity. This effect of monensin could even improve the clinical outcome in patients with NASH-related HCC, by killing cancer cells and mitigating steatosis, which might extend the liver function, raising the necessity of further studies to determine its effects on metabolic pathways involved in lipid metabolism regulation. The in vitro observations on the reduction of steatosis by monensin and on the lack of effects of PA on monensin cytotoxicity were obtained in preliminary experiments and need to be confirmed and more deeply investigated.

In agreement to what previously reported in the allograft models of breast cancer and HCC [44,45], Monensin exerts no anti-proliferative activity in normal but also in steatotic HCC cells (C1C7 cells pretreated or not with Palmitic Acid). This can predict better safety profile and less serious adverse effects when compared to chemotherapies.

These findings have important translational implications. First, monensin's ability to simultaneously target multiple hallmarks of cancer (angiogenesis, metabolism, and immune evasion) makes it an attractive candidate for HCC therapy. Second, its FDA-approved status and established safety profile could facilitate rapid clinical translation. Future studies should explore the precise mechanisms linking Na+ dysregulation to immune modulation, how monensin reduces steatosis, and potential synergies between monensin and immunotherapies.

In conclusion, this study positions monensin as a unique multimodal therapeutic agent for HCC, capable of inducing direct tumor cytotoxicity while simultaneously remodeling the tumor microenvironment to favor antitumor immunity. These effects, combined with its favorable safety profile, suggest that monensin warrants clinical evaluation as both a monotherapy and potential combination partner in HCC treatment strategies.

7. Bibliography

1. Cancer Today (2022). Globocan. https://gco.iarc.who.int/today/.

2. Llovet, J.M., Kelley, R.K., Villanueva, A., Singal, A.G., Pikarsky, E., Roayaie, S., Lencioni, R., Koike, K., Zucman-Rossi, J., and Finn, R.S. (2021). Hepatocellular carcinoma. Nat. Rev. Dis. Primer *7*, 6. https://doi.org/10.1038/s41572-020-00240-3.

3. Koshy, A. (2025). Evolving Global Etiology of Hepatocellular Carcinoma (HCC): Insights and Trends for 2024. J. Clin. Exp. Hepatol. *15*. https://doi.org/10.1016/j.jceh.2024.102406.

4. medscape, medscape (2024). Hepatocellular Carcinoma (HCC): Practice Essentials, Anatomy, Pathophysiology. https://emedicine.medscape.com/article/197319-overview.

5. Zhang, T., Nie, Y., and Wang, J. (2023). The emerging significance of mitochondrial targeted strategies in NAFLD treatment. Life Sci. *329*, 121943. https://doi.org/10.1016/j.lfs.2023.121943.

6. Huang, D.Q., El-Serag, H.B., and Loomba, R. (2021). Global epidemiology of NAFLD-related HCC: trends, predictions, risk factors and prevention. Nat. Rev. Gastroenterol. Hepatol. *18*, 223–238. https://doi.org/10.1038/s41575-020-00381-6.

7. Bayard, Q., Meunier, L., Peneau, C., Renault, V., Shinde, J., Nault, J.-C., Mami, I., Couchy, G., Amaddeo, G., Tubacher, E., et al. (2018). Cyclin A2/E1 activation defines a hepatocellular carcinoma subclass with a rearrangement signature of replication stress. Nat. Commun. *9*, 1–14. https://doi.org/10.1038/s41467-018-07552-9.

8. K, S., S, I., E, L., Lb, A., J, C., S, R., G, C., C, M., J, S., F, S., et al. (2015). Exome sequencing of hepatocellular carcinomas identifies new mutational signatures and potential therapeutic targets. Nat. Genet. *47*. https://doi.org/10.1038/ng.3252.

9. Guichard, C., Amaddeo, G., Imbeaud, S., Ladeiro, Y., Pelletier, L., Maad, I.B., Calderaro, J., Bioulac-Sage, P., Letexier, M., Degos, F., et al. (2012). Integrated analysis of somatic mutations and focal copy-number changes identifies key genes and pathways in hepatocellular carcinoma. Nat. Genet. *44*, 694–698. https://doi.org/10.1038/ng.2256.

10. Dy, C., A, V., Y, H., J, P., P, N., B, M., Ac, L., Dj, D., Sn, T., M, S., et al. (2008). Focal gains of VEGFA and molecular classification of hepatocellular carcinoma. Cancer Res. *68*. https://doi.org/10.1158/0008-5472.CAN-08-0742.

11. Wang, Y., and Deng, B. (2023). Hepatocellular carcinoma: molecular mechanism, targeted therapy, and biomarkers. Cancer Metastasis Rev. *42*, 629–652. https://doi.org/10.1007/s10555-023-10084-4.

12. Bialecki, E.S., and Di Bisceglie, A.M. (2005). Diagnosis of hepatocellular carcinoma. HPB *7*, 26–34. https://doi.org/10.1080/13651820410024049.

13. Ayuso, C., Rimola, J., Vilana, R., Burrel, M., Darnell, A., García-Criado, Á., Bianchi, L., Belmonte, E., Caparroz, C., Barrufet, M., et al. (2018). Diagnosis and staging of hepatocellular carcinoma (HCC): current guidelines. Eur. J. Radiol. *101*, 72–81. https://doi.org/10.1016/j.ejrad.2018.01.025.

14. RONCALLI, M. (2009). Pathologic diagnosis of early hepatocellular carcinoma : a report of the international consensus group for hepatocellular neoplasia. https://air.unimi.it/handle/2434/49917.

15. Reig, M., Forner, A., Rimola, J., Ferrer-Fàbrega, J., Burrel, M., Garcia-Criado, Á., Kelley, R.K., Galle, P.R., Mazzaferro, V., Salem, R., et al. (2022). BCLC strategy for prognosis prediction and treatment recommendation: The 2022 update. J. Hepatol. *76*, 681–693. https://doi.org/10.1016/j.jhep.2021.11.018.

16. Makary, M.S., Khandpur, U., Cloyd, J.M., Mumtaz, K., and Dowell, J.D. (2020). Locoregional Therapy Approaches for Hepatocellular Carcinoma: Recent Advances and Management Strategies. Cancers *12*, 1914. https://doi.org/10.3390/cancers12071914.

17. Niu, M., Yi, M., Li, N., Wu, K., and Wu, K. (2021). Advances of Targeted Therapy for Hepatocellular Carcinoma. Front. Oncol. *11*, 719896. https://doi.org/10.3389/fonc.2021.719896.

18. Li, M., Bhoori, S., Mehta, N., and Mazzaferro, V. (2024). Immunotherapy for hepatocellular carcinoma: The next evolution in expanding access to liver transplantation. J. Hepatol. *81*, 743–755. https://doi.org/10.1016/j.jhep.2024.05.037.

19. Hepa-1c1c7 (ECACC 95090613). Cult. Collect. https://www.culturecollections.org.uk/nop/product/hepa-1c1c7.

20. Sundi, P.R.I.O., Thipe, V.C., Omar, M.A., Adelusi, T.I., Gedefa, J., and Olaoba, O.T. (2024). Preclinical human and murine models of hepatocellular carcinoma (HCC). Clin. Res. Hepatol. Gastroenterol. *48*, 102418. https://doi.org/10.1016/j.clinre.2024.102418.

21. Lee, J., Cho, Y.S., Kim, J., Shim, Y.M., Lee, K.-H., and Choi, J.Y. (2021). Prognostic Significance of Metabolic Parameters by 18F-FDG PET/CT in Thymic Epithelial Tumors. Cancers *13*, 712. https://doi.org/10.3390/cancers13040712.

22. Gu, C.Y., and Lee, T.K.W. (2022). Preclinical mouse models of hepatocellular carcinoma: An overview and update. Exp. Cell Res. *412*, 113042. https://doi.org/10.1016/j.yexcr.2022.113042.

23. Connor, F., Rayner, T.F., Aitken, S.J., Feig, C., Lukk, M., Santoyo-Lopez, J., and Odom, D.T. (2018). Mutational landscape of a chemically-induced mouse model of liver cancer. J. Hepatol. *69*, 840–850. https://doi.org/10.1016/j.jhep.2018.06.009.

24. Memon, A., Pyao, Y., Jung, Y., Lee, J.I., and Lee, W.K. (2020). A Modified Protocol of Diethylnitrosamine Administration in Mice to Model Hepatocellular Carcinoma. Int. J. Mol. Sci. *21*, 5461. https://doi.org/10.3390/ijms21155461.

25. Ajith, A., Mulloy, L.L., Musa, M.A., Bravo-Egana, V., Horuzsko, D.D., Gani, I., and Horuzsko, A. (2021). Humanized Mouse Model as a Novel Approach in the Assessment of Human Allogeneic Responses in Organ Transplantation. Front. Immunol. *12*. https://doi.org/10.3389/fimmu.2021.687715.

26. Wenzel, N., Blasczyk, R., and Figueiredo, C. (2021). Animal Models in Allogenic Solid Organ Transplantation. Transplantology *2*, 412–424. https://doi.org/10.3390/transplantology2040039.

27. Graves, S.S., Parker, M.H., and Storb, R. (2018). Animal Models for Preclinical Development of Allogeneic Hematopoietic Cell Transplantation. ILAR J. *59*, 263–275. https://doi.org/10.1093/ilar/ily006.

28. Boursier, J., Hagström, H., Ekstedt, M., Moreau, C., Bonacci, M., Cure, S., Ampuero, J., Nasr, P., Tallab, L., Canivet, C.M., et al. (2022). Non-invasive tests accurately stratify patients with NAFLD based on their risk of liver-related events. J. Hepatol. *76*, 1013–1020. https://doi.org/10.1016/j.jhep.2021.12.031.

29. Li, M.O., Wolf, N., Raulet, D.H., Akkari, L., Pittet, M.J., Rodriguez, P.C., Kaplan, R.N., Munitz, A., Zhang, Z., Cheng, S., et al. (2021). Innate immune cells in the tumor microenvironment. Cancer Cell *39*, 725–729. https://doi.org/10.1016/j.ccell.2021.05.016.

30. Ratziu, V., Rinella, M., Beuers, U., Loomba, R., Anstee, Q.M., Harrison, S., Francque, S., Sanyal, A., Newsome, P.N., and Younossi, Z. (2020). The times they are a-changin' (for NAFLD as well). J. Hepatol. *73*, 1307–1309. https://doi.org/10.1016/j.jhep.2020.08.028.

31. Ma, C., Kesarwala, A.H., Eggert, T., Medina-Echeverz, J., Kleiner, D.E., Jin, P., Stroncek, D.F., Terabe, M., Kapoor, V., ElGindi, M., et al. (2016). NAFLD causes selective CD4+ T lymphocyte

loss and promotes hepatocarcinogenesis. Nature *531*, 253–257. https://doi.org/10.1038/nature16969.

32. Pilmis, B., Kherabi, Y., Huriez, P., Zahar, J.-R., and Mokart, D. (2023). Infectious Complications of Targeted Therapies for Solid Cancers or Leukemias/Lymphomas. Cancers *15*, 1989. https://doi.org/10.3390/cancers15071989.

33. Drochioiu, G. (2023). Multifactorial Distress, the Warburg Effect, and Respiratory and pH Imbalance in Cancer Development. Stresses *3*, 500–528. https://doi.org/10.3390/stresses3020036.

34. Ouwerkerk, R., Bleich, K.B., Gillen, J.S., Pomper, M.G., and Bottomley, P.A. (2003). Tissue sodium concentration in human brain tumors as measured with 23Na MR imaging. Radiology *227*, 529–537. https://doi.org/10.1148/radiol.2272020483.

35. Carini, R., De Cesaris, M.G., Bellomo, G., and Albano, E. (1999). Intracellular Na+ accumulation and hepatocyte injury during cold storage. Transplantation *68*, 294–297. https://doi.org/10.1097/00007890-199907270-00023.

36. PubChem Monensin Sodium. https://pubchem.ncbi.nlm.nih.gov/compound/23690927.

37. Aowicki, D., and Huczyński, A. (2013). Structure and antimicrobial properties of monensin A and its derivatives: summary of the achievements. BioMed Res. Int. *2013*, 742149. https://doi.org/10.1155/2013/742149.

38. Serter Kocoglu, S., Oy, C., Secme, M., and Sunay, F.B. (2023). Investigation of the anticancer mechanism of monensin via apoptosis-related factors in SH-SY5Y neuroblastoma cells. Clin. Transl. Sci. *16*, 1725–1735. https://doi.org/10.1111/cts.13593.

39. Wang, X., Wu, X., Zhang, Z., Ma, C., Wu, T., Tang, S., Zeng, Z., Huang, S., Gong, C., Yuan, C., et al. (2018). Monensin inhibits cell proliferation and tumor growth of chemo-resistant pancreatic cancer cells by targeting the EGFR signaling pathway. Sci. Rep. *8*, 17914. https://doi.org/10.1038/s41598-018-36214-5.

40. Zhou, Y., Deng, Y., Wang, J., Yan, Z., Wei, Q., Ye, J., Zhang, J., He, T.-C., and Qiao, M. (2023). Effect of antibiotic monensin on cell proliferation and IGF1R signaling pathway in human colorectal cancer cells. Ann. Med.

41. Yao, S., Wang, W., Zhou, B., Cui, X., Yang, H., and Zhang, S. (2021). Monensin suppresses cell proliferation and invasion in ovarian cancer by enhancing MEK1 SUMOylation. Exp. Ther. Med. *22*, 1–10. https://doi.org/10.3892/etm.2021.10826.

42. Kim, S.-H., Kim, K.-Y., Yu, S.-N., Park, S.-G., Yu, H.-S., Seo, Y.-K., and Ahn, S.-C. (2016). Monensin Induces PC-3 Prostate Cancer Cell Apoptosis via ROS Production and Ca2+ Homeostasis Disruption. Anticancer Res. *36*, 5835–5843.

43. Clemente, N., Baroni, S., Fiorilla, S., Tasso, F., Reano, S., Borsotti, C., Ruggiero, M.R., Alchera, E., Corrazzari, M., Walker, G., et al. (2023). Boosting intracellular sodium selectively kills hepatocarcinoma cells and induces hepatocellular carcinoma tumor shrinkage in mice. Commun. Biol. *6*, 574. https://doi.org/10.1038/s42003-023-04946-4.

44. Fiorilla, S., Tasso, F., Clemente, N., Trisciuoglio, T., Boldorini, R., and Carini, R. (2025). Monensin Inhibits Triple-Negative Breast Cancer in Mice by a Na+-Dependent Cytotoxic Action Unrelated to Cytostatic Effects. Cells *14*, 185. https://doi.org/10.3390/cells14030185.

45. Clemente, N., Baroni, S., Fiorilla, S., Tasso, F., Reano, S., Borsotti, C., Ruggiero, M.R., Alchera, E., Corrazzari, M., Walker, G., et al. (2023). Boosting intracellular sodium selectively kills hepatocarcinoma cells and induces hepatocellular carcinoma tumor shrinkage in mice. Commun. Biol. *6*, 574. https://doi.org/10.1038/s42003-023-04946-4.

46. Shirakami, Y., Gottesman, M.E., and Blaner, W.S. (2012). Diethylnitrosamine-induced hepatocarcinogenesis is suppressed in lecithin:retinol acyltransferase-deficient mice primarily through retinoid actions immediately after carcinogen administration. Carcinogenesis *33*, 268–274. https://doi.org/10.1093/carcin/bgr275.

47. Santos, N.P., Pereira, I.C., Pires, M.J., Lopes, C., Andrade, R., Oliveira, M.M., Colaço, A., Peixoto, F., and Oliveira, P.A. (2012). Histology, bioenergetics and oxidative stress in mouse liver exposed to N-diethylnitrosamine. Vivo Athens Greece *26*, 921–929.

48. Barral, M., Raballand, A., Dohan, A., Soyer, P., Pocard, M., and Bonnin, P. (2016). Preclinical Assessment of the Efficacy of Anti-Angiogenic Therapies in Hepatocellular Carcinoma. Ultrasound Med. Biol. *42*, 438–446. https://doi.org/10.1016/j.ultrasmedbio.2015.10.012.